TASK QUARTERLY 5 No 4 (2001), 479–496

NUMERICAL SIMULATION OF 3D VISCOUS TURBOMACHINERY FLOW WITH HIGH-RESOLUTION ENO SCHEME AND MODERN TURBULENCE MODEL

SERGEY V. YERSHOV[1,2] AND ANDREY V. RUSANOV[1,2]

[1] *FlowER Ltd,*
1/27 Akhsarov, 310202 Kharkov, Ukraine
yershov@flower3d.org, http:/www.flower3d.org

[2] *Institute of Mechanical Engineering Problems,*
National Academy of Sciences of Ukraine,
2/10 Pozharsky, 310046 Kharkov, Ukraine
yershov@online.kharkiv.com

(Received 20 July 2001; revised manuscript received 15 August 2001)

Abstract: This paper presents the basic principles of construction of numerical models for 3D viscous turbulent flows through multi stage turbomachines. The great attention is given to such properties of the methods as accuracy, linear and non-linear stability, robustness and computational efficiency. It is shown that these properties can be guaranteed if the implicit Godunov's type ENO scheme is used. A 3D code **FlowER** has been developed within this concept. Using the code the numerical results are obtained for flows through high loaded compressor cascades, a turbine stage, a low-pressure multi stage turbine and a centrifugal compressor stage. The results of optimisation of a low-pressure turbine last stage are presented.

Keywords:

1. Introduction

The last twenty years are marked by quick development of the computational fluid dynamics (CFD). On the one hand the progress in this field was caused by the necessity to solve new tasks of aerodynamics but on the other, it became possible due to truly fantastic growth of computing power. This progress also affected turbomachinery CFD. Figure 1 displays the main changes which occurred over the last years in the field of simulation of turbomachinery flows.

Up to quite a recent time, flows through isolated cascades or stages have been considered. Often the two-dimensional flow model was used. The flows were usually described by Euler equations which were solved either by second-order accurate central-difference schemes with artificial viscosity or by first-order accurate upwind schemes. Such approaches cannot ensure the accurate simulation and robustnes of the algorithms. In most cases we can rely on qualitative simulation only.

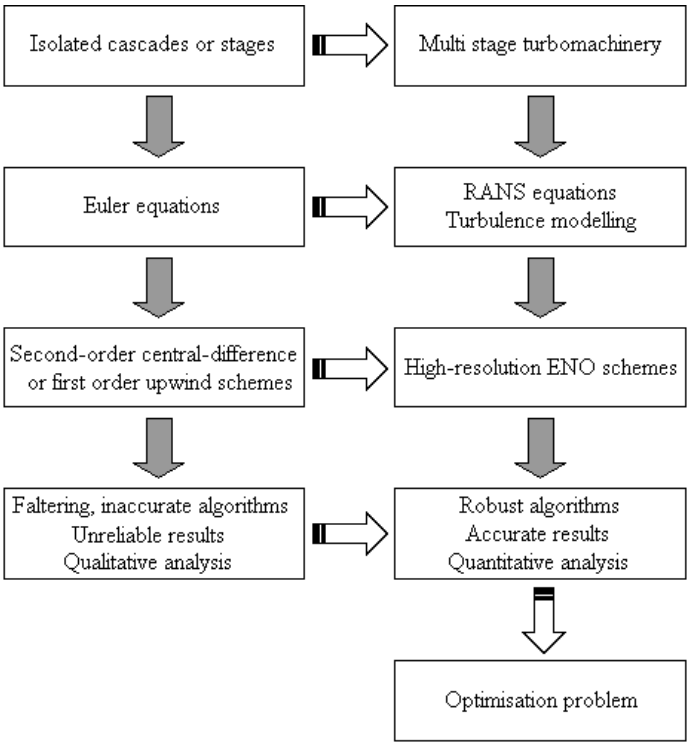

Figure 1. Progress in turbomachinery CFD

The modern problem statement considers 3D viscous throughflow in multi stage turbomachine as a whole. The 3D Reynolds-averaged Navier-Stokes (RANS) equations are solved numerically for these purposes. The turbulent effects are simulated with advanced turbulence models. The governing equations are numerically integrated with high-resolution ENO schemes of second (or higher) order of accuracy and it is possible to obtain mathematically accurate and physically valid results for a wide range of flow parameters. We can perform quantitative simulation in CFD now. Robustness, reliability and computational efficiency of numerical algorithms have grown so much that CFD solvers can be used for blade shape optimisation.

In the present paper the basic principles of modern approach of numerical simulation of 3D viscous turbomachinery flows are described.

2. Multi stage turbomachinery flow model

As it has been noted the advanced problem statement considers the model of flow through multi stage turbomachinery including axial and radial elements (Figure 2). For successful simulation the model must describe all basic properties of the flow under consideration, in particular compressibility, viscosity, 3D effects, unsteadiness, effects caused by various design features of turbomachine, namely radial gap flow, leakages *etc.* The 3D RANS equations are deemed to be the minimum possible level of the models to simulate these properties and effects. Today the flow models based on more simple Euler equations as well as 2D models can be considered as artefacts of the past century. At best they can be used as proof ground for new numerical technologies.

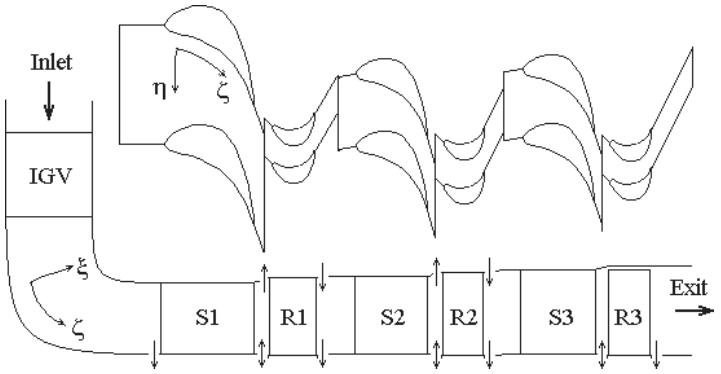

Figure 2. Computational domain

The RANS equations can be written for a local curvilinear body-fitted coordinate system [1] in the form suitable for numerical integration:

$$\frac{\partial QJ}{\partial t}+\frac{\partial\left(E\xi_x+F\xi_y+G\xi_z\right)J}{\partial\xi}+\frac{\partial\left(E\eta_x+F\eta_y+G\eta_z\right)J}{\partial\eta}+\frac{\partial\left(E\zeta_x+F\zeta_y+G\zeta_z\right)J}{\partial\zeta}=HJ, \quad (1)$$

where $Q=\begin{bmatrix}\rho\\ \rho u\\ \rho v\\ \rho w\\ h\end{bmatrix}$ is vector of conservative variables; $E=\begin{bmatrix}\rho u\\ \rho u^2+p-\tau_{xx}\\ \rho uv-\tau_{xy}\\ \rho uw-\tau_{xz}\\ (h+p)u-u\tau_{xx}-v\tau_{xy}-w\tau_{xz}+q_x\end{bmatrix}$,

$F=\begin{bmatrix}\rho v\\ \rho uv-\tau_{xy}\\ \rho v^2+p-\tau_{yy}\\ \rho vw-\tau_{yz}\\ (h+p)v-u\tau_{xy}-v\tau_{yy}-w\tau_{yz}+q_y\end{bmatrix}$, $G=\begin{bmatrix}\rho w\\ \rho uw-\tau_{xz}\\ \rho vw-\tau_{yz}\\ \rho w^2+p-\tau_{zz}\\ (h+p)w-u\tau_{xz}-v\tau_{yz}-w\tau_{zz}+q_z\end{bmatrix}$ are flux vectors; $H=\begin{bmatrix}0\\ 2\rho v\Theta+\rho\Theta^2 r_x\\ -2\rho u\Theta+\rho\Theta^2 r_y\\ 0\\ 0\end{bmatrix}$ is vector of source terms; $h=\frac{p}{\gamma-1}+\frac{u^2+v^2+w^2-\Theta^2\boldsymbol{r}^2}{2}$;

$\tau_{ij}=\tau_{mij}+\tau_{tij}$; $\tau_{mij}=2\mu_m\left(S_{ij}-S_{nn}\delta_{ij}/3\right)$; $\tau_{tij}=2\mu_t\left(S_{ij}-S_{nn}\delta_{ij}/3\right)-2\rho k\delta_{ij}/3$; $\lambda=\lambda_m+\lambda_t=c_p(\mu_m/\mathrm{Pr}_m+\mu_t/\mathrm{Pr}_t)$; p, ρ, u, v, w are pressure, density and velocity components; Θ is rotational speed of local curvilinear co-ordinate system (ξ,η,ζ); τ_{mij}, τ_{tij}, τ_{ij} are tensors of laminar, turbulent and total viscous stresses; S_{ij} is mean strain rate tensor; $T=p/(\rho R)$ is temperature; μ, μ_m, μ_t are coefficients of viscosity, molecular viscosity and turbulent viscosity; λ, λ_m, λ_t are thermal conductivity, molecular thermal conductivity and turbulent thermal conductivity; Pr_m, Pr_t are laminar and turbulent Prandtl numbers; $\boldsymbol{q}=-\lambda\nabla T$ is heat flux; $\boldsymbol{r}$ is radius vector. Here and below the subscripts i,j take values 1, 2, 3, which correspond to Cartesian coordinate axes x, y, z. It is suitable for numerical solution to present the viscous stress tensor and the heat flux in curvilinear coordinates too. The RANS Equations (1) can be written for multi-component and multi-phase flows as well as for an arbitrary equation of state but in the present paper the case of perfect gas is only considered.

3. Turbulence modelling

The Navier-Stokes equations are generally assumed to completely simulate the turbulent phenomena occurring in the flow. However, to ensure such simulation it is necessary to use extremely refined grids sufficient for resolution of small-scale turbulent vortices. According to this, the direct numerical simulation of turbulence for engineering purposes is a task of a far future. Up to date using this approach and supercomputers the only results that have worked out were simple simulative solutions [2–4]. For the same reason, the development turned out to be retarded for another promising approach, namely large-eddy simulation (LES) [1, 5], which assumes the direct calculation of large-scale vortices only, whereas the small-scale (subgrid) vortices are simulated. Therefore the main direction of CFD progress, so far, is the solution of the RANS Equations (1). The RANS equations are not closed; therefore it is necessary to simulate turbulent effects using turbulence models.

The development of advanced turbulence models is one of the main tasks of today. Accuracy and reliability of simulation of elementary turbulent effects determine the accuracy of computations of such flow phenomena as separation, laminar-turbulent transition, wakes, boundary layers *etc.*

Although the first investigations of turbulent flows began more than one hundred years ago, the results in this field are not as impressive as wanted. Moreover, it is considered that universal adequate models simpler than Navier-Stokes equations themselves are impossible [6]. Therefore appearance of new more accurate turbulence models [7, 8] is encouraging.

Up to now CFD solvers have used mainly algebraic [9, 10] or two-equation [11–13] models of turbulent viscosity. The basic common drawback of these models is insufficient accuracy for flows with high adverse pressure gradients. The most popular k-ε turbulence model [12] must be especially considered. Some terms that are important near walls were omitted in equations, and the model, which performs well for free stream, is incorrect for more or less complicated wall flows with pressure gradient [14–16]. Recently many modifications of two-equations turbulent models have been suggested. According to opinion of some investigators [17, 18], today the shear-stress transport (SST) model developed by Menter [7] is among the most promising ones. The SST model combining k-ε and k-ω ones inherits the best features of them. The SST model equations can be written as follows:

$$\frac{\partial UJ}{\partial t}+\frac{\partial(R_x\xi_x+R_y\xi_y+R_z\xi_z)J}{\partial\xi}+\frac{\partial(R_x\eta_x+R_y\eta_y+R_z\eta_z)J}{\partial\eta}+ +\frac{\partial(R_x\zeta_x+R_y\zeta_y+R_z\zeta_z)J}{\partial\zeta}=(G-D+L)J; \tag{2}$$

where $U=\begin{bmatrix}\rho k\\ \rho\omega\end{bmatrix}$; $R_i=\begin{bmatrix}\rho k-(\mu+\mu_t/\sigma_k)\dfrac{\partial k}{\partial x_i}\\ \rho\omega-(\mu+\mu_t/\sigma_\omega)\dfrac{\partial\omega}{\partial x_i}\end{bmatrix}$; $G=\begin{bmatrix}\tau_{tij}S_{ij}\\ \gamma\rho\Omega^2\end{bmatrix}$; $D=\begin{bmatrix}\beta^*\rho\omega k\\ \beta\rho\omega^2\end{bmatrix}$;

$L=\begin{bmatrix}0\\ 2(1-F_1)\dfrac{\rho}{\omega\sigma_{\omega2}}\dfrac{\partial k}{\partial x_i}\dfrac{\partial\omega}{\partial x_i}\end{bmatrix}$; $\mu_t=\dfrac{\rho k/\omega}{\max\left(1;\Omega F_2/(\alpha\omega)\right)}$; $F_1=\mathrm{th}\left(\left(\min\left(A_1;A_2\right)\right)^4\right)$;

$A_1=\max(B_1;B_2)$; $A_2=\dfrac{4\rho k}{C_{k\omega}\sigma_{\omega2}n^2}$; $F_2=\mathrm{th}\left(\left(\max(2B_1;B_2)\right)^2\right)$; $B_1=\dfrac{\sqrt{k}}{\beta^*\omega n}$; $B_2=\dfrac{\mu}{\rho n^2\omega}$;

$\varphi=F_1\varphi_1+(1-F_2)\varphi_2$; $\varphi=[\sigma_k,\sigma_\omega,\beta,\gamma]$; $\Omega=\sqrt{\frac{1}{2}\Omega_{ij}\Omega_{ij}}$; $\Omega_{ij}=\dfrac{\partial u_i}{\partial x_j}-\dfrac{\partial u_j}{\partial x_i}$; $S_{ij}=\dfrac{\partial u_i}{\partial x_j}+\dfrac{\partial u_j}{\partial x_i}$;

k is turbulent kinetic energy; ω is specific turbulent dissipation rate (turbulent frequency); Ω is magnitude of mean vorticity; n is distance to the nearest wall. The constants of the model are the following: $\alpha = 0.31$; $\beta^* = 0.09$; $\sigma_{k1} = 1.176$; $\sigma_{k2} = 1.0$; $\sigma_{\omega 1} = 2.0$; $\sigma_{\omega 2} = 1.168$; $\beta_1 = 0.075$; $\beta_2 = 0.0828$; $\gamma_1 = 0.553$; $\gamma_2 = 0.44$. The major feature of the SST model is switching from k-ε model in freestream to k-ω one near walls. The softness of the switching is provided by the blending function F_1. The definition of turbulent eddy viscosity in the model is based on Bradshaw's assumption that the principal shear stress is proportional to the turbulent kinetic energy over most part of the boundary layer. This definition improves the prediction of flows with strong adverse pressure gradients and separation. The function F_2 is included to prevent the singular behaviour of the model in the freestream where the vorticity can vanish.

4. Boundary conditions

Specification of boundary conditions for the RANS equations is more or less difficult.

The number of boundary conditions at the inlet and exit permeable boundaries is determined by the characteristic analysis. To calculate the flow parameters at the boundary points, the compatibility relations or extrapolation are applied. This definition is supplemented by the "soft" conditions for derivatives of velocity components and temperature.

At walls the impermeability condition is imposed. Besides it is necessary to specify the heat flux or wall temperature. The wall pressure is usually determined from the following equality for transverse pressure gradient

$$\frac{\partial p}{\partial n} = 0,$$

that is true for thin infinite boundary layers. For a more accurate pressure definition it is necessary to use relations derived from Navier-Stokes equations [19]:

$$\frac{\partial p}{\partial \eta} = \eta_0^2 \frac{\partial}{\partial \eta}\left(\frac{\mu}{J}\frac{\partial V^* J}{\partial \eta}\right) + \frac{1}{3}\frac{\partial}{\partial \eta}\left(\frac{\mu}{J}\frac{\partial V J}{\partial \eta}\right) + \rho\Omega^2\left(r_x x_\eta + r_y y_\eta\right), \tag{3}$$

where $V^*/J = (ux_\eta + vy_\eta + wz_\eta)/J$ is covariant velocity component that corresponds to the grid cross-direction η. If $r \perp \eta$ then the last term in Equation (3) is identically equal to zero.

Sometimes one can use the so-called "reflection" conditions according to which the computational domain is supplemented by "ghost" cells. The pressure and density in these cells are imposed to be equal to those in the adjacent "real" cells whereas the opposite sign is assigned to the velocity components. Careful analysis shows that "reflection" conditions are incorrect since they are true only for boundary layers and in general case they contradict the Navier-Stokes equations.

Two-equation turbulence models require imposing additional boundary conditions.

At no-slip surfaces turbulence kinetic energy is considered to be equal to zero, $k = 0$. The turbulent frequency at walls is determined from the asymptotic relation [7]:

$$\omega = \frac{60\mu_w}{\rho_w \beta n_1^2},$$

where n_1 is the normal distance from the wall to the nearest cell centre.

At the inlet it is necessary to specify two additional parameters, namely the turbulent kinetic energy k and turbulent frequency ω. Imposing the turbulence kinetic energy k turns out to be convenient enough since it can directly be tied to the inlet turbulence intensity Tu as:

$$k = 1.5\,(Tu \cdot U_\infty)^2, \tag{4}$$

where U_∞ is the velocity of external flow at the inlet.

At the same time, imposing the inlet turbulent frequency sometimes leads to insuperable obstructions, since neither theoreticians nor engineers know what it must be equal to. Often instead of turbulent frequency, ω, one specifies the turbulence scale, which is more physically representable but is no more a univocal quantity. It is evident that such boundary conditions for ω have serious drawbacks. Firstly, quantities k and ω, specified in such a way, generally correspond to a non-equilibrium turbulence state therefore the appreciable alteration of turbulent flow is expected near the inlet boundary. In the issue the turbulent intensity of changed inlet flow can essentially differ from the specified one. Secondly, this approach does not take into account the effect of inlet boundary layers. Thirdly, as it has been noted, the turbulent frequency and turbulence scale are the quantities that cannot be determined with required accuracy for real flows.

In the present paper it is proposed to determine the inlet boundary condition for ω from the local equilibrium of turbulence. The inlet turbulent frequency can be determined from Equations (2) as:

$$\omega = \sqrt{\frac{\max\left(S\Omega, \Omega^2\right)}{\beta^*}}, \tag{5}$$

where $S = \sqrt{\frac{1}{2} S_{ij} S_{ij}}$. The quantity $\tau_{ij} S_{ij}/\mu_t$ in Equation (5) is changed by Ω^2 (Menter's assumption [7, 20, 18]) or by $S\Omega$ (hypothesis of Kato and Launder [21]).

The kinetic energy of turbulence at the boundary layer can be represented as $k = l^2 \Omega\omega$ [22], where $l = \min(\kappa y, \beta^* \delta)$ is mixing length, $\kappa = 0.41$ is Kármán constant, δ is boundary layer thickness. Combining this representation with Equation (4) yields finally:

$$k = \max\left(\tfrac{3}{2}\left(Tu \cdot U_\infty\right)^2, l^2\,\Omega\omega\right). \tag{6}$$

The use of Equations (4)–(6) as the inlet boundary conditions for the SST turbulent model is very convenient and leads to good results.

5. Difference scheme

The choice of a difference scheme is a key issue, and unfortunately insufficient attention is often given to this question although the bad choice of a scheme can reduce to nothing any attempt to achieve more or less feasible results. The difference schemes must satisfy many acknowledged requirements.

The most important of these requirements are displayed in Figure 3. Firstly it is necessary to demand the accuracy of approximation. Practical experience in solving complex CFD problems shows that at least *second-order accurate* schemes are preferable. Such choice is motivated by the fact that the first-order accurate schemes used for nonlinear equations at irregular grids can introduce the error which cannot be eliminated by

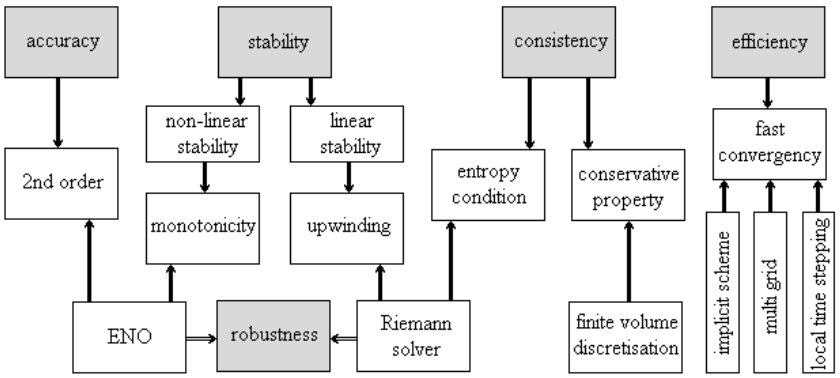

Figure 3. Principal requirements for difference schemes

grid refinement [23]. At present the first-order accurate schemes are not used for serious investigations [24].

At the same time formally high scheme accuracy by itself means nothing if the scheme is not stable enough or is not stable at all. The scheme stability is determined largely by the manner of approximation of convective derivatives. It is a well-known fact that the downwind approximation leads to absolutely unstable schemes. On the contrary, the *upwind schemes* are known to be highly stable. The central-difference schemes are intermediate in their properties; usually they are not stable enough even in the linear sense. The evident explanation of this fact is that the upwind schemes are compatible with zones of influence in the flow but other schemes are not. For the reason mentioned above, it is advisable to use upwind schemes only.

The *non-linear stability* of the scheme is greatly important in the first place for transonic and supersonic flow computations. It is well known that the excessive numerical dispersion attending high-order accurate schemes can lead to spurious oscillations in the regions with high flow gradients. Often in this case the convergence of the solution is generally not achieved with the grid refinement [25]. Even if the oscillation amplitude is not large and reduces with the grid refinement, it is difficult to use the solutions obtained to determine flow derivatives, shock positions *etc.* Moreover, the oscillations pinch on flow field processing and analysis of computational results. In the worst case the solution failure is possible at intensive shocks and expansion waves. Therefore it is desirable to use the *monotonicity-preserving* schemes. Ensuring this property and second-order accuracy simultaneously is possible with ENO reconstruction only.

The next important requirement is the scheme *consistency*. We would like to consider this property in a wider sense than usually. Difference scheme consistency may not only be a correspondence of difference approximation to original difference equations and to as many of their corollaries as possible (*e.g.* conservation laws in various notations). The consistency of the scheme with fundamental physical laws, such as the second law of thermodynamics, is very important. Thus the scheme is consistent if it is at least *conservative* and satisfies the *entropy condition* [26]. For the flows with strong discontinuities the use of non-conservative schemes leads to the significant errors at finite grids. The conservative property of the scheme is ensured by the control volume technique.

If the scheme does not satisfy the entropy condition then the numerical solutions can be incorrect, in particular non-physical expansion shock is possible! It is necessary to note that even for fully subsonic flows the zones with reduced entropy can be observed if one uses the scheme that does not satisfy the entropy condition. Such behaviour of numerical solution fatally corrupts an estimation of losses in the flow. The correct solution of the problem consists in the construction of the schemes with entropy enforcement that satisfies the entropy condition. The *Godunov's Riemann solver* that selects physical solutions [27] turns out to ensure both, the scheme upwinding property and entropy enforcement.

The *robustness* of a scheme also plays a pivotal role. Besides, if the CFD solver is designed for optimisation problems then it is necessary to guarantee fail-safety of the software for an arbitrary computational domain geometry and computational grid. Otherwise, the determination of an optimal solution can be impossible.

The monotonicity preserving upwind schemes are known to be robust. On the contrary, the non-monotonous schemes behave "capriciously", which leads to negative values of pressure and density at intensive shocks and expansion waves. In such cases the continuation of computations is either impossible at all or makes no sense. Thus the ENO scheme using the Godunov's Riemann solver turns out to satisfy automatically the robustness.

The computations of high Reynolds number turbulent flows require very fine grids with refinement near walls. It leads to an increase in computational time. Insufficient *computational efficiency* of a difference scheme can hamper the usage of software if one flow computation takes a few tens or hundreds of hours on high performance computers. Therefore often it is not efficient to use *explicit* schemes. The *implicit* schemes permit the significant increase of a time step and as a result acceleration of the convergence. Therefore the latter are more preferable. Besides, various convergence accelerators such as multi grid techniques, local time stepping can be used if it is possible.

Unfortunately one often ignores such important scheme properties as monotonicity-preserving, upwinding and entropy conditions. In this case the artificial viscosity is declared to be a remedy for all numerical troubles. However, the addition of artificial viscosity inevitably leads to a decrease in accuracy. If artificial viscosity is commensurable with the physical one a correct estimation of losses is not possible. It is especially unpleasant that the artificial viscosity does not completely eliminate numerical troubles, which evoke it! Incompletely smoothed oscillations and zones with reduced entropy often mark the obtained solutions. Besides, the stability of schemes with artificial viscosity is worse than that of the upwind monotonicity-preserving ones.

On a balance, we can conclude that the use of the second order-accurate implicit ENO scheme based on Godunov's Riemann solver is the most advisable at present. The first such scheme appears to be suggested by Yershov [28, 29].

An increment of conservative variables δQ at time step τ is determined by volume integration of Equations (1) over cell (i,j,k):

$$\begin{aligned}\delta Q^{n+1}_{i,j,k} = Q^{n+1}_{i,j,k} - Q^{n}_{i,j,k} = -\frac{\tau}{\left(\Delta\xi\,\Delta\eta\,\Delta\zeta\,J\right)_{i,j,k}}\Big(&\left(E^n\,\Delta\eta\Delta\zeta\right)_{i+\frac{1}{2},j,k} - \left(E^n\,\Delta\eta\Delta\zeta\right)_{i-\frac{1}{2},j,k}\\ &+\left(F^n\,\Delta\xi\,\Delta\zeta\right)_{i,j+\frac{1}{2},k} - \left(F^n\,\Delta\xi\,\Delta\zeta\right)_{i,j-\frac{1}{2},k}\\ &+\left(G^n\,\Delta\xi\,\Delta\eta\right)_{i,j,k+\frac{1}{2}} - \left(G^n\,\Delta\xi\,\Delta\eta\right)_{i,j,k-\frac{1}{2}}\Big) + \tau\,H^n_{i,j,k}\,, \qquad (7)\end{aligned}$$

where $\Delta\xi$, $\Delta\eta$ and $\Delta\zeta$ are spatial steps. Equation (7) represents finite difference equations in the finite volume form and therefore it ensures conservative property of a solution.

The fluxes E, F and G at the cell surfaces are calculated with Godunov's Riemann solver [27], which ensures upwind differencing and enforcement of entropy condition [26]. Initial values for the Riemann solver are calculated with spatial-temporal interpolation of primitive variables q as follows:

$$q(\xi,\eta,\zeta,t) = q_m^n + \left(\overline{\frac{\partial q}{\partial \xi}}\right)_m^n (\xi-\xi_m) + \left(\overline{\frac{\partial q}{\partial \eta}}\right)_m^n (\eta-\eta_m) + \left(\overline{\frac{\partial q}{\partial \zeta}}\right)_m^n (\zeta-\zeta_m), \tag{8}$$

where subscript m corresponds to the centre of a current cell.

Equations (7) and (8) define a wide family of locally second-order schemes [30, 31, 23] (*etc.*) differing in ways of approximation of derivatives $\overline{\partial\phi/\partial\psi}$. The monotonocity-preserving uniformly second-order accurate scheme can be built with ENO reconstruction for characteristic variables ϕ [29]:

$$\Delta_m \phi = L_\psi \Delta_m q; \tag{9}$$

$$\left(\overline{\frac{\partial \phi}{\partial \psi}}\right)_m^n = \frac{1}{\Delta\psi}\operatorname{minmod}\big[\Delta_m\phi + \alpha\operatorname{minmod}(\Delta_m\phi - \Delta_{m-1}\phi, \Delta_{m+1}\phi - \Delta_m\phi), \Delta_{m+1}\phi - \beta\operatorname{minmod}(\Delta_{m+1}\phi - \Delta_m\phi, \Delta_{m+2}\phi - \Delta_{m+1}\phi)\big]; \tag{10}$$

$$\left(\overline{\frac{\partial q}{\partial \psi}}\right)_m^n = L_\psi^{-1}\left(\overline{\frac{\partial \phi}{\partial \psi}}\right)_m^n, \tag{11}$$

where ψ is grid direction ξ, η or ζ; $\Delta_m q = q_m - q_{m-1}$; L_ψ is matrix of left eigenvectors of Jacobian of Equations (1); α and β are constants, minmod function is defined as:

$$\operatorname{minmod}(a,b) = \operatorname{sign}(a)\max\Big(0, \min\big(|a|, b\operatorname{sign}(a)\big)\Big). \tag{12}$$

For $\alpha+\beta=1$ in particular $\alpha=\beta=\frac{1}{2}$, we have an ENO scheme that is uniformly second-order accurate in time and space. For $\alpha = 2\beta = \frac{2}{3}$, the scheme is locally third-order accurate, remaining at least second-order everywhere. The irregular grid requires to correct Equation (10) for non-uniform spatial steps as well as to adjust coefficients α and β to take into account a spatial step size and a direction of disturbance propagation.

The computational efficiency of the scheme (7)–(12) can be increased by an implicit operator presented in δ-form [29]. The implicit step can be represented as a sequence of matrix transformations performed with the conservative variable vector δQ, obtained after the explicit step (7):

1) transformation to primitive variables

$$\delta q^n = \frac{1}{1+\chi} T \delta Q^n + \frac{\chi}{1+\chi}\delta q^{n-1}; \tag{13}$$

2) transformation to characteristic variables with regards to coordinate ξ

$$\delta \phi_\xi^n = L_\xi \delta q^n; \tag{14}$$

3) implicit step with regards to ξ

$$\left(I + \frac{\tau\theta}{(1+\chi)J}\frac{\partial}{\partial\xi}\left(\Lambda_\xi^+ + \Lambda_\xi^-\right)\right)\delta\phi_\xi^{n+\frac{1}{3}} = \delta\phi_\xi^n; \tag{15}$$

4) inverse transformation to primitive variables

$$\delta q^{n+\frac{1}{3}} = L_\xi^{-1}\delta\phi_\xi^{n+\frac{1}{3}} \tag{16}$$

5) transformation to characteristic variables with regards to coordinate η

$$\delta\phi_{\eta}^{n+\frac{1}{3}} = L_{\eta}\delta q^{n+\frac{1}{3}} \tag{17}$$

6) implicit step with regards to η

$$\left(I + \frac{\tau\theta}{(1+\chi)J}\frac{\partial}{\partial\eta}\left(\Lambda_{\eta}^{+} + \Lambda_{\eta}^{-}\right)\right)\delta\phi_{\eta}^{n+\frac{2}{3}} = \delta\phi_{\eta}^{n+\frac{1}{3}}; \tag{18}$$

7) inverse transformation to primitive variables

$$\delta q^{n+\frac{2}{3}} = L_{\eta}^{-1}\delta\phi_{\eta}^{n+\frac{2}{3}} \tag{19}$$

8) transformation to characteristic variables with regards to coordinate ζ

$$\delta\phi_{\zeta}^{n+\frac{2}{3}} = L_{\zeta}\delta q^{n+\frac{2}{3}} \tag{20}$$

9) implicit step with regards to ζ

$$\left(I + \frac{\tau\theta}{(1+\chi)J}\frac{\partial}{\partial\zeta}\left(\Lambda_{\zeta}^{+} + \Lambda_{\zeta}^{-}\right)\right)\delta\phi_{\zeta}^{n} = \delta\phi_{\zeta}^{n+\frac{2}{3}}; \tag{21}$$

10) inverse transformation to primitive variables

$$\delta q^{n} = L_{\zeta}^{-1}\delta\phi_{\zeta}^{n} \tag{22}$$

11) calculation of primitive variables in a subsequent time step $n+1$

$$q^{n+1} = q^{n} + \delta q^{n}. \tag{23}$$

The Equations (7)–(23) represent the high-resolution implicit ENO scheme used in the code **FlowER**.

6. Grid construction

Traditional approaches of construction of structural grids for computational domains with complex geometry encounter serious difficulties, which can sometimes be insuperable. There are two different ways to solve the nascent problems. The first of them consists in changing from structured rectangular grids to the unstructured triangular ones. The drawbacks of this approach are evident. On the one hand, the numerical algorithms become extremely complicated since there is no general way to tie the index of an arbitrary cell with neighbouring cell indexes. It leads to the significant increase of computational expenses. On the other hand, numerical schemes based on triangular grids are characterized by the larger scheme diffusion than the analogous ones with traditional grids. The grid refinement near walls leads to extremely elongated cells and generates additional large irreducible errors.

The second approach consists in the use of composition of blocks with rectangular grids. For complicated computational domains, the blocks can be disposed irregularly and in this case the computational grid is disordered as a whole but structured for each block in itself. The main drawback of this approach is always deemed to consist in the reduction of accuracy caused by the use of interpolations and truncated stencils at the boundaries of adjacent blocks. Rusanov [32, 33] has suggested new computational technology, namely the algorithm of uniform multi block calculation (UMC), according to which there are no computational differences between internal cells and those at the permeable boundaries of blocks. Owing to the splitting of difference equations, the computational process under

this technology ensures thorough calculations along grid lines at each step of numerical integration. Therefore UMC algorithms are equal in accuracy to traditional structural grid ones and are not computationally expensive. One implementation of this approach is given in [33]. More advanced implementation of the UMC algorithm developed is being tested now.

7. Numerical simulation of 3D viscous turbomachinery flow

7.1. Rotor37

In the first place, numerical results concerning 3D flow through Rotor37 cascade will be considered. It is a highly loaded compressor cascade (pressure ratio is 2.1) with high rotation velocity (17188 rpm), large Mach numbers (up to 1.8) and low stability margin (less than 8 per cent of the flow rate from the choking condition). The flow through Rotor37 is characterized by intensive shock waves and massive separation over a wide range of conditions.

The flows through high-loaded compressor cascades still remain extremely difficult for numerical simulations. This is largely due to non-adequacy of most turbulence models for flows with adverse pressure gradient that tend to yield unrealistic massive separations. Mainly due to these peculiarities, the computation of Rotor37 flow is the admitted test for numerical methods [24]. According to the opinion of many CFD experts the code that had not successfully passed a test with Rotor37 flow should not be used for design purposes.

The Mach number contours at the midspan section for the choking condition are displayed in Figure 4a. The complicated flow pattern is observed to include reflected and closure shocks as well as bow shocks. The Mach number contours at midspan section for 98% flow condition are given in Figure 4b. It is clearly seen that the bow and closure shocks combine and form a single strong shock in this case. The flow at suction side separates after the shock. Numerical results show that the lower the mass flow rate the larger the separation region. In the issue it causes the loss of stability. The present results are in good agreement with experimental data [34].

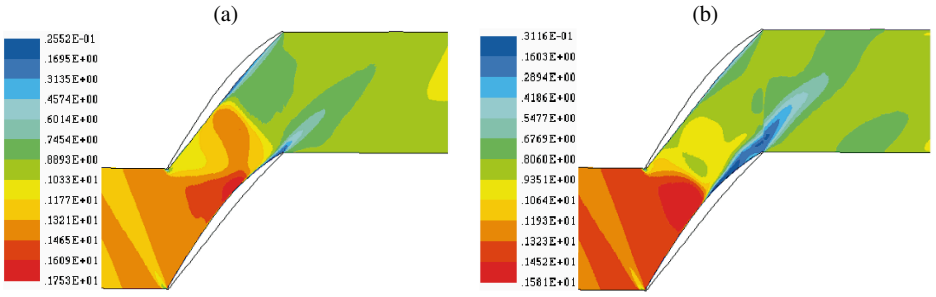

Figure 4. Mach number contours at midspan section of Rotor37:
(a) choking condition; (b) 98% of choking mass flow rate

The total pressure ratio as a function of mass flow rate is presented in Figure 5 (top). Here the results obtained experimentally and numerically by other authors are compared with the present computations. The analogous plot is given for adiabatic efficiency in Figure 5 (bottom). The measurement error is shown in both plots [34]. The numerical results obtained with code **FlowER** are seen to be in good agreement with experimental data.

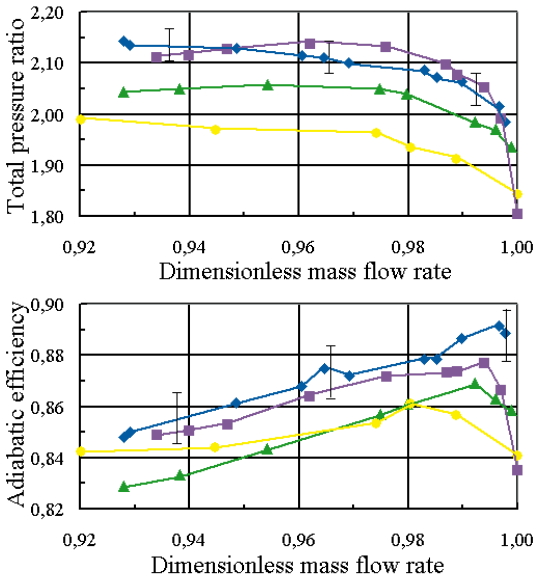

Figure 5. Total pressure ratio and adiabatic efficiency for Rotor37: ◆ experiment [34]; ■ **FlowER**; ▲ Hirsch and Kang [35]; ● Denton and Xu [34]

It should be emphasized that the use of algebraic turbulence models (such as Baldwin-Lomax model [9]) for simulation of Rotor37 flow leads to significant difficulties, which are caused by non-adequacy of these models for separations and adverse pressure gradients. Most likely the correct simulation of the near stall condition with algebraic models is not possible at all.

7.2. *Compressor cascade K11*

Analogous results can be presented for other compressor cascades [36]. The Mach number contours at K11 cascade [20] are presented in Figure 6a for calculations using the Baldwin-Lomax algebraic turbulence model. The extended separation zones are observed at the suction and pressure sides of the blade. As a result the flow cannot reach high speed and the maximum Mach number at the suction side is about 1. The application of the SST model reduces the extension of the separation zone (Figure 6b). The maximum Mach number at the suction side for this case is about 1.27, which is in good agreement with the result obtained with code TASKFLOW at Aviadvigatel Ltd, Perm, Russia [20].

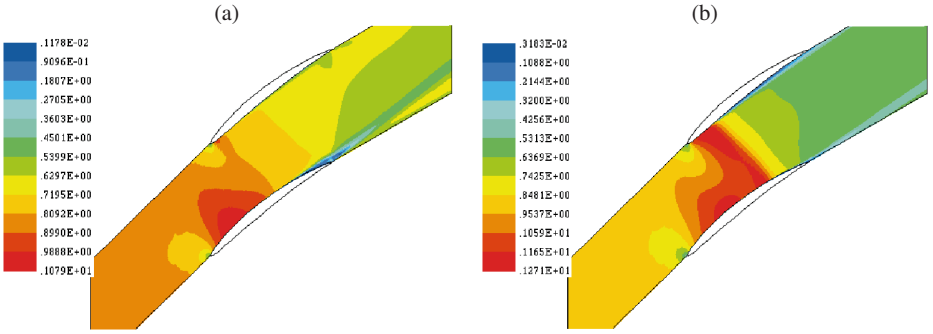

Figure 6. Mach number contours for K11 cascade

7.3. Gas turbine stage

Similar tendencies are observed for transonic flow within turbine cascades [36]. The Mach number contours at the midspan section of the gas turbine stator are given in Figure 7. The computation using the Baldwin-Lomax model (Figure 7a) shows non-physically large separation. The SST model gives more realistic results (Figure 7b). Reciprocally, in the last case the flow at the suction side of the blade reaches higher speed and it results in a more intensive and sharp shock wave. The analysis of numerical data shows interesting properties for the results obtained with the SST model. The secondary flows are characterized by larger intensity. The secondary vortices are disposed closer to the endwalls and more compact.

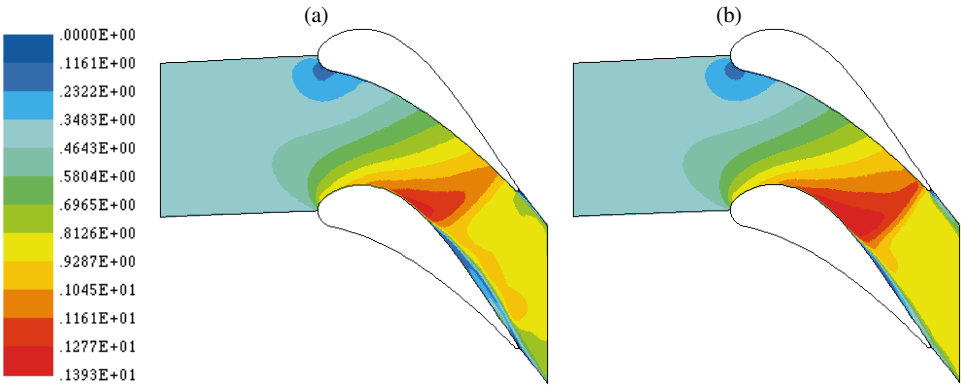

Figure 7. Mach number contours at midspan section of gas turbine stator

7.4. Low pressure multi stage turbine

The computation of throughflow within low-pressure multi stage turbine has also been performed. The first turbine stator was installed so that the through flow it is radial. The velocity vectors at the midpitch meridional section of the flowpath are presented in Figure 8. Enlarged fragments of the turbine passage are shown for regions of extractions and leakages.

7.5. Centrifugal compressor

The viscous flow through a three-row centrifugal compressor is considered [37]. The compressor comprises a centrifugal wheel, radial vaned diffuser and (converse) radial vaned diffuser (Figure 9).

The velocity vectors for the midpitch meridional section of the flowpath are displayed in Figure 9. As it is seen from the picture, the flow pattern is complex enough. The generation of separations and vortices is observed in the flow. We can suppose that the geometry of hub and tip endwalls is far from optimal near the channel bend where the massive separation origins. This separation influences flow far downstream. The flow in converse vaned diffuser leaves off being uniform and the stagnation zones appear around the main flow jet. It is evident that such a flow structure is characterized by high losses.

It should also be stated that the secondary flows of centrifugal wheels are more complex than those of the axial ones. In the first place, it is evidenced by generation of passage vortices not only at tip and case endwalls but also at the pressure and suction sides of the blades. It is evoked by the existence of both circumferential pressure gradient and spanning one in the rotor blade-to-blade passage. The entropy contours for different

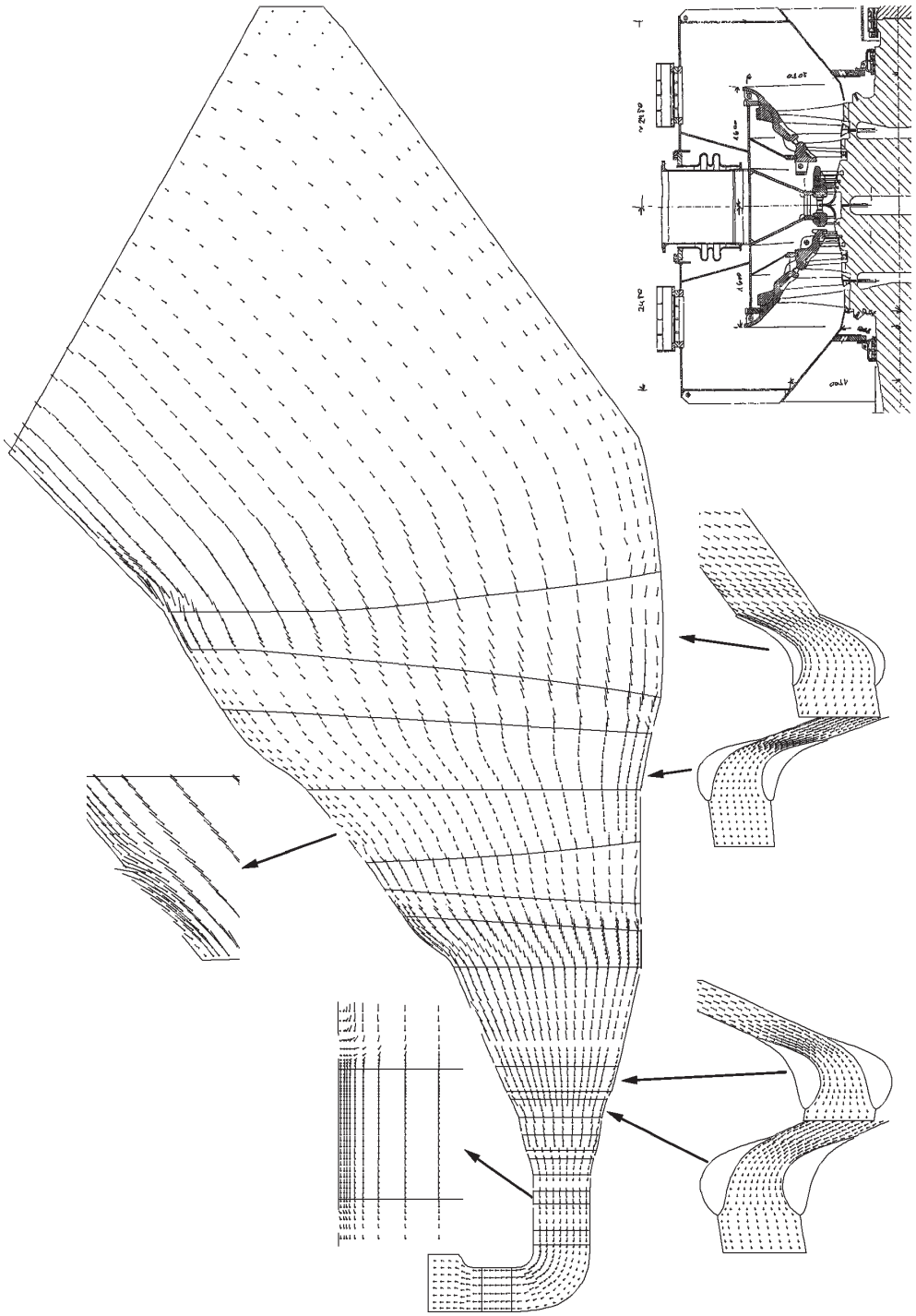

Figure 8. Velocity vectors at midpitch meridional section of low pressure multi stage turbine

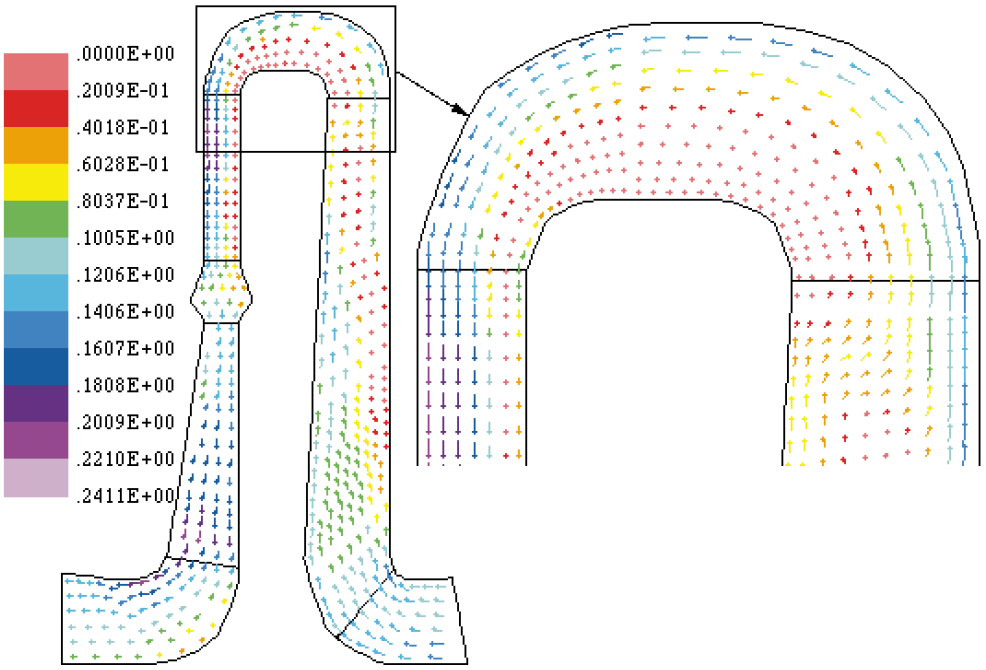

Figure 9. The velocity vectors at the midpitch section of three-row centrifugal compressor

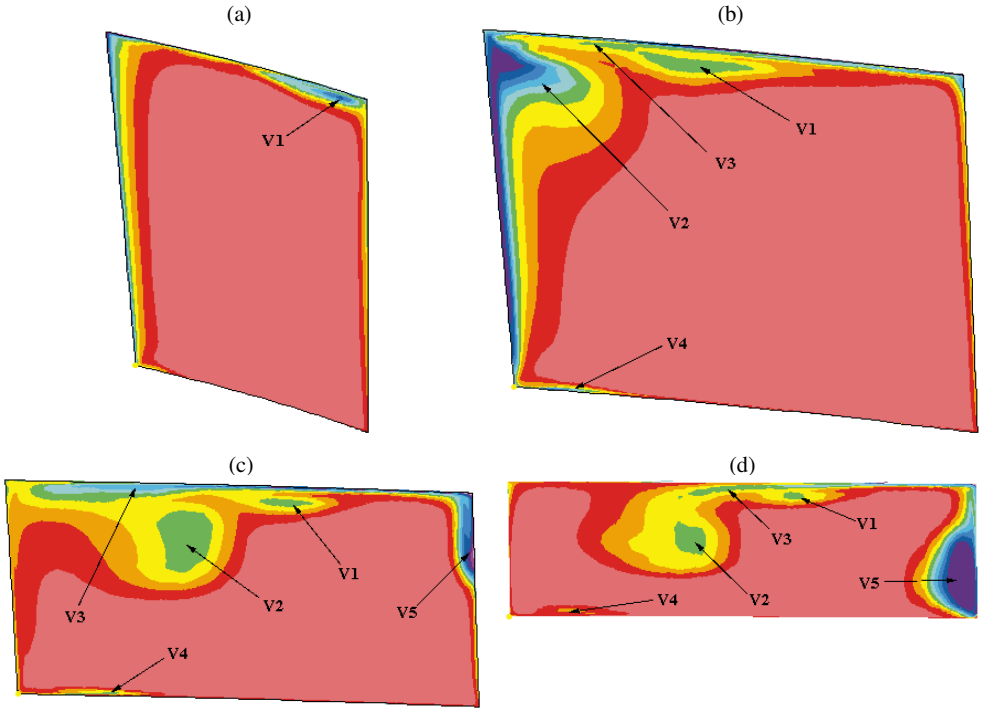

Figure 10. Entropy function contours for cross-flow sections of rotor (percentage of chord): (a) – 9%; (b) – 34%; (c) – 59%; (d) – 86%

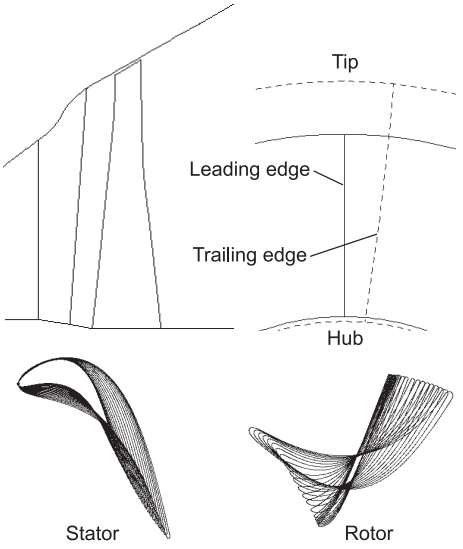

Figure 11. Initial stage

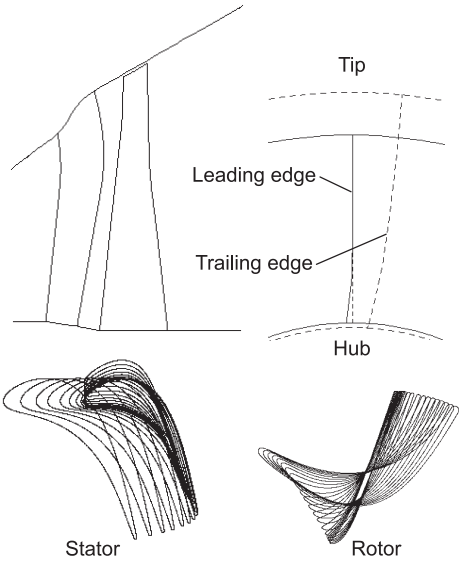

Figure 12. Modified CLS stage

cross-flow sections of the wheel vane channel are presented in Figure 10. One can estimate the location of vortices by the position of local maxima of the entropy. The analysis of flow pattern permits us to describe the following main vortices: the branch of tip horseshoe vortex v1, the pressure side passage vortex v2, the tip passage vortex v3, the root passage vortex v4, the suction side passage vortex v5. The other branches of root and tip horseshoe vortices are not seen in Figure 10 since they have merged with the passage vortices and due to their small intensity and coarse picture scale.

7.6. Optimisation

The high accuracy and robustness of the solver **FlowER** permit us to use it successfully for optimisation problems [38]. In the present paper the optimisation of a low-pressure exit turbine stage is considered as an example. The initial shape of stage blades is shown in Figure 11. The stator blade generatrices were straight lines for the initial stage. The following geometrical parameters were varied, stagger angles of the stator and rotor, lean and sweep angles of the stator, two parameters of stator compound sweep at the tip and two parameters of stator compound lean at the hub.

The shape of the blades for the optimised stage with compound lean and sweep of the stator blade (CLS stage) is shown in Figure 12. For this stage the efficiency increase at design conditions is almost 1.2 per cent. The dependence of stage efficiency on the mass flow rate is given in Figure 13 for the initial stage (solid line) and for CLS stage (dashed line). Here, the results for a modified stage with straight lean and sweep of stator blade (SLS stage) are displayed too (dotted line). The CLS stage is more efficient for design at high load conditions. The SLS stage is more efficient for low load conditions. For the conditions with the mass flow equal to 26 kg/s the increase of efficiency is about 10.9 per cent for CLS stage and it is approximately 14.3 per cent for the SLS stage.

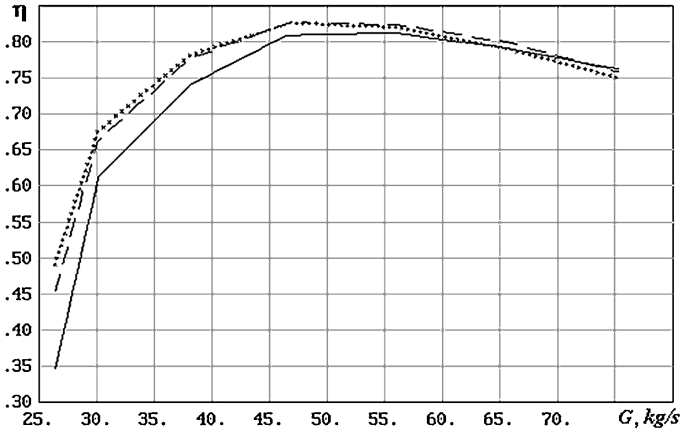

Figure 13. Efficiency of stage versus mass flow rate: solid line – initial stage; dashed line – CLS stage; dotted line –SLS stage

8. Conclusion – prospects of numerical models of 3D viscous turbomachinery flows

Finally we would like to note the main promising directions of turbomachinery CFD development. Firstly the advanced numerical methods must be extended on a working medium with a sufficiently arbitrary equation of state, also on multi-component and multi-phase flows.

The growth of computer power allows the calculation of flow through composite aerodynamic devices (such as air-engine) on the whole taking into account the small details of geometry. It must necessarily entail the solution of multidisciplinary problems that involve aerodynamics, heat transfer, aeroelasticity, combustion *etc.*

The developed CFD solvers will be included in more and more complex optimisation algorithms. It is also necessary to say about the further improvement of turbulence models. In the first place, it concerns the refinement of laminar-turbulent transition and wall flows with pressure gradients.

Although the accuracy of advanced numerical methods is good enough for many engineering goals, the improvement of difference schemes is and will be one of the main problems of CFD. Modern DES, LES and DNS techniques require developing the high-order accuracy schemes (more than fourth-order accurate) and solving the problems caused by enlargement of the approximation stencils.

References

[1] Fletcher C A J 1988 *Computational Techniques for Fluid Dynamics* Springer-Verlag, p. 1056
[2] Kim J, Moin P and Moser R 1987 *J. Fluid Mech.* **177** 133
[3] Kristoffersen R and Andersson H I 1993 *J. Fluid Mech.* **256** 163
[4] Rodi W and Mansour N N 1993 *J. Fluid Mech.* **250** 509
[5] Huai X, Joslin R D and Piomelli U 1997 *Large-Eddy Simulation of Laminar-Turbulent Transition in a Swept-Wing Boundary Layer* AIAA Paper 97-0750, p. 11
[6] Singer B A 1993 *Modeling the Transition Region* NASA CR 4492, p. 88
[7] Menter F R 1994 *AIAA Journal* **32** (11) 1299
[8] Spalart P R and Allmaras S R 1992 *A One-Equation Turbulence Model for Aerodynamic Flows* AIAA Paper 92-0439, p. 11

[9] Baldwin B S and Lomax H 1978 *Thin Layer Approximation and Algebraic Model for Separated Turbulent Flows* AIAA Paper 78–257, p. 8
[10] Michel R, Quémard C and Durant R 1969 *Aplication d'un schema de longeur de mélange a l'étude des couches limites turbulentes d'équilibre* ONERA TN 154, p. 11
[11] Coakley T J 1983 *Turbulence Modeling Methods for the Compressible Navier-Stokes Equations* AIAA Paper 83-1693, p. 12
[12] Launder B E and Sharma B I 1974 *Letters in Heat and Mass Transfer* **1** (2) 131
[13] Wilcox D C 1988 *AIAA Journal* **26** (11) 1299
[14] Huang P G and Bradshaw P 1995 *AIAA Journal* **33** (4) 624
[15] Takemitsu N 1990 *J. Fluid Mech.* **112** (6) 192
[16] Yoon B K and Chung M K 1995 *AIAA Journal* **33** (8) 1518
[17] Bardina J E, Huang P G and Coakley T J 1997 *Turbulence Modeling Validation, Testing, and Development* NASA TM–110446, p. 98
[18] Forsythe J R, Strang W Z and Hoffmann K A 2000 *Validation of Several Reynolds-Averaged Turbulence Models in a 3-D Unstructured Grid Code* AIAA Paper 00–2552, p. 20
[19] Yershov S V and Rusanov A V 1998 *J. Mechanical Engineering* **1** (1) 70 (in Russian)
[20] Bratukhin A G, Reshetnikov Y E and Inozemtsev A A 1999 *Designing And Manufacturing Gas Turbine Engines For Airliners* Moscow, Aviatechinform, p. 554 (in Russian)
[21] Kato M and Launder B E 1993 *The Modeling of Turbulent Flow around Stationary and Vibrating Square Cylinders* Proc. 9th Symposium on Turbulent Shear Flows, Kyoto, August 1993, 10.4.1–10.4.6
[22] Lai K Y M and Makomaski A H 1989 *J. Fluids Engineering* **69** (4) 449
[23] Tillyayeva N I 1986 *Scientific Acta of Central Aerogasdynamical Institute* **17** (2) 18 (in Russian)
[24] Yershov S V 1998 *J. Mechanical Engineering* **1** (2) 76 (in Russian)
[25] Yee H C, Warming R F and Harten A 1985 *Lectures in Applied Mathematics* **22** 357
[26] Harten A 1983 *J. Comput. Phys* **49** (3) 357
[27] Godunov S K 1976 *Numerical Solution of Multidimensional Problems of Gasdynamics* Nauka, Moscow p. 400 (in Russian)
[28] Yershov S V 1991 *Problems in Machinery* **35** 77 (in Russian)
[29] Yershov S V 1994 *Mathematical Modelling* **6** (11) 63 (in Russian)
[30] Eidelman S, Colella P and Shreeve R P 1984 *AIAA Journal* **22** (11) 1609
[31] Kolgan V P 1972 *Scientific Acta of Central Aerogasdynamical Institute* **3** (6) 68 (in Russian)
[32] Rusanov A V, Solodov V G, Starodubtsev Yu V and Yershov S V 2001 *The Uniform Numerical Technique For Multiblock CFD Solver* Proc. 5th Internat. Symp. Aerothermodynamics of Internal Flows, Sept. 2001, Gdańsk, Poland (will be published)
[33] Rusanov A V, Yershov S V and Kudrinski A V 1998 *The Uniform Algorithms for Calculation of Flow through Composite Arbitrary Domains* Proceedings of 3rd Congress of Engine Engineers of Ukraine with Foreign Participation, Kharkov, Kharkov Aerospace University, pp. 100–103 (in Russian)
[34] Denton J D 1996 *Lessons from Rotor37* Proc. 3*rd* Internat. Symp. Aerothermodynamics of Internal Flows, Sept. 1996, Beijing, China 3–14
[35] Kang S and Hirsch C 1997 *NASA Compressor Rotor37 Test Case, 3D Flow Simulation in Turbomachinery* The ERCOFTAC Seminar and Workshop, 6–10 January 1997, Courchevel, France, pp. 1–10
[36] Yershov S V, Rusanov A V and Shapochka A Yu 2001 *3D Viscous Transonic Turbomachinery Flows: Numerical Simulation and Optimisation Using Code* **FlowER** Proc. 5th Internat. Symp. Aerothermodynamics of Internal Flows, Sept. 2001, Gdańsk, Poland (will be published)
[37] Yershov S V and Rusanov A V 1999 *J. Mechanical Engineering* **2** (1–2) 27 (in Russian)
[38] Yershov S V, Shapochka A Yu and Rusanov A V 2000 *J. Mechanical Engineering* **3** (3–4) 21 (will be published) (in Russian)